Separation Science and Technology
Publication details, including instructions for authors and subscription information:
http://www.informaworld.com/smpp/title~content=t713708471

Sorption Modeling of Strontium, Plutonium, Uranium, and Neptunium Adsorption on Monosodium Titanate

F. F. Fondeur[a]; D. T. Hobbs[a]; S. D. Fink[a]; M. J. Barnes[a]
[a] Westinghouse Savannah River Company, Aiken, SC, USA

To cite this Article Fondeur, F. F. , Hobbs, D. T. , Fink, S. D. and Barnes, M. J.(2005) 'Sorption Modeling of Strontium, Plutonium, Uranium, and Neptunium Adsorption on Monosodium Titanate', Separation Science and Technology, 40: 1, 571 — 592
To link to this Article: DOI: 10.1081/SS-200042517
URL: http://dx.doi.org/10.1081/SS-200042517

Separation Science and Technology, 40: 571–592, 2005
ISSN 0149-6395 print/1520-5754 online
DOI: 10.1081/SS-200042517

Sorption Modeling of Strontium, Plutonium, Uranium, and Neptunium Adsorption on Monosodium Titanate

F. F. Fondeur, D. T. Hobbs, S. D. Fink, and M. J. Barnes
Westinghouse Savannah River Company, Aiken, SC, USA

Abstract: We examined the ability of various equilibrium isotherms to replicate the available data for the adsorption of strontium (Sr), plutonium (Pu), uranium (U), and neptunium (Np) on monosodium titanate (MST) during the treatment of simulated and actual Savannah River Site high-level waste. The data come from numerous experimental studies conducted between 1999 and 2002. The analysis considered 29 isotherm models from the literature. As part of this study, we developed a general method for selecting the best isotherm equation. The selection criteria for rating the isotherm equations considered the relative error in predicting the experimental data, the complexity of the mathematical expressions, the thermodynamic validity of the expressions, and statistical significance for the expressions.

The Fowler Guggenheim-Jovanovic Freundlich (FG-JF), the Fowler Guggenheim-Langmuir Freundlich (FG-LF) and the Dubinin-Astashov (DA) isotherms each reliably predicted the actinide and Sr adsorption on MST. The first two models describe the adsorption process by single layer formation and lateral interactions between adsorbed sorbates, while the DA model assumes volume filling of micropores (by osmotic pressure difference). These two mechanisms include mutually exclusive assumptions. However, we cannot determine which model best represents the various adsorption mechanisms on MST. Based on our analysis, the DA model predicted the data well. The DA model assumes that an initial sorption layer forms after which networking begins in the pore spaces, filling the volume by a second mechanism. If this mechanism occurs in MST, as the experimental data suggest, then we expect all the empty and closed spaces of MST to contain actinides and Sr when saturated. Prior microstructure analyses determined that the MST surface is best described as heterogeneous (i.e., a semicrystalline outer layer on an amorphous

Address correspondence to F. F. Fondeur, Westinghouse Savannah River Company, Aiken, SC 29808, USA. E-mail: fernando.fondeur@srs.gov

core) or composite material for adsorption. Therefore, we expect the empty spaces (of nanometer size) between the crystalline units in the fibrous material to provide sorption area for the actinides and Sr. Additional conclusions from this study follow.

Since each of the three models work reliably, we recommend use of the computationally simplest model as the primary tool until future work can differentiate between the two mechanisms. The DA model possesses a simpler mathematical form with fewer parameters and operations.

The experimental data for actual and simulated wastes generally showed consistent agreement. However, the data sets do include considerable variance from a number of causes including the following:

- The Pu sorption data appear most consistent (e.g., between actual and simulated waste) and most easily predicted. Since Pu removal efficiency proves most important for the process design efforts, this consistency of the data proves especially beneficial.
- Extremely high mass loadings of U on MST result in multilayer sorption behavior and divergence from classical single monolayer isotherm forms. Prior X-ray studies demonstrate that U begins to network, or form dimers, which agrees with this interpretation. This U behavior also shows a complex interaction, and a direct correlation, with sorption data for the other radionuclides. We believe these data suggest nucleation (e.g., precipitation) of the actinides in the micropore space for both Np and Pu. For Sr, the high U loadings appear to inhibit the sorption of Sr.
- Nearly all the solutions contained U as the radionuclide with the highest mass concentration. These data show the widest variance.
- The composite data set indicates a notable variance in sorption for different batches of MST. The sorption of Sr with different batches of MST shows the largest variance among the four radionuclides for different batches of MST. This variance remains a relatively unexplored aspect of the process design.
- Similarly, the experimental data included a wide variety of solution compositions. As such, the mathematical expressions implicitly account for variances in solution chemistry typical of that anticipated within the Salt Waste Processing Facility and Actinide Removal Process. The reader must consider the ranges of these concentrations when applying the expressions.
- Increasing temperature decreases Sr, Pu, and, to a lesser extent, U sorption on MST. The opposite effect occurs with Np. This temperature variance further suggests a nucleation behavior for Np.
- Nearly all the data used in developing the sorption models came from experiments using solutions with all the principle radionuclides of interest present simultaneously. We modeled the data without invoking competition between the actinides and Sr despite the large concentrations of both U and Np. Since the model does not explicitly invoke competition, the optimized parameters implicitly carry the impact of interaction within the concentration ranges of the original data. Hence, extrapolation of the models to concentrations markedly outside those ranges may result in poorer predictive ability.

INTRODUCTION

The Salt Waste Processing Facility that is to be built at the Savannah River Site (SRS) includes adsorption as a unit operation for removing traces of

alpha- and beta-emitting elements from the waste solution. The facility uses monosodium titanate (MST) for strontium (Sr) and actinide removal. In particular, the objective of the process is the removal of Sr (90), plutonium (Pu 238 and 239), and neptunium (Np 237) with MST. A number of batch contacting experiments were conducted to obtain information on the kinetics and capacity of the media. The tests demonstrated the ability of MST to remove both Sr and the actinides from alkaline solutions containing up to 90,000 times as much sodium as sorbate (on a molar basis).

These tests identified the need for additional scientific work to understand the interaction between the actinides and MST. Recently, Savannah River Technology Center (SRTC) personnel conducted X-ray scattering experiments such as Extended X-rays Adsorption Fine Structure (EXAFS) and Transmission Electron Microscopy (TEM) on MST (1). The analysis indicated MST is an amorphous, spherical particle (with average diameter of about 4 to 5 microns) coated with about 150 to 500 nanometers of a crystalline and fibrous material. The fibrous material contains distorted titanium oxide octahedra. An Energy Dispersive Spectrometry (EDS) in a TEM scan of the fibrous layer of S-loaded MST indicated that Sr tends to adsorb on the fibrous layer of MST. The studies could not definitively identify the physical location of the actinides within the microstructure due to the low-detection limits for these elements and their lower relative concentrations. The structural studies identified the differing nature of the surface chemistry for the various radionuclides. These findings include the following:

- Presence of titanium (Ti) in the second coordination shell of the Sr^{2+} on the MST suggests that specific adsorption is the predominant mechanism and that electrostatic bonding (also known as ion exchange of hydrated surface-associated species such as dissolved Na^{+}) in the electric double layer of the HLW salt simulant solution does not occur.
- Uranium(VI) sorbs via an inner sphere/specific adsorption mechanism as predominantly dimeric nitrato or carbonato complexes of U(VI) species via bidentate linkages (i.e., assuming the presence of Ti octahedra in the MST structure, the U(VI) is bound to Ti groups at two different U-Ti radial distances) at high loadings. Monomeric species predominate at low loadings.
- Plutonium, added as Pu(IV), exhibits inner sphere/specific adsorption as polymeric (colloidal) Pu species—with a local environment that is consistent with Pu(IV).
- Neptunium, from salt solutions spiked with a Np(V) stock solution, exhibits inner sphere specific adsorption as polymeric Np species. The Np may be present as Np(V) or Np(IV).

From these spectroscopy and scattering work conclusions, the actinides of interest and Sr bind specifically to MST. Therefore, we can neglect

nonspecific or electrostatic adsorption as described by the Diffuse Double Layer, Triple Layer, Capacitance Layer, Debye-Huckel, and Donnan Theories. This work focused only on specific adsorption as described by isotherms.

For successful implementation of MST, the adsorption process needs to use an optimal amount of MST and must remain predictable under plant-upset conditions. These studies provide, for the first time, sufficient data to derive a model for predicting such performance.

Adsorption is a general term that refers to the disappearance of solutes from solutions with the presumption of adsorption to a solid surface. The accumulation of solutes at the solid–liquid interface results from physical or chemical interactions with the surface. Physical bonding is relatively weak, while chemical bonding is a stronger interaction which may involve ionic or covalent bonding (in addition to van der Waals and London forces). The nature of both the solid surface and the solute determines the interaction.

Inorganic surfaces consist of mostly oxygen and hydroxides. In high pH (very caustic solutions), the inorganic surfaces are mainly oxygen anions. Exchangeable cations (e.g., alkali metals such as Li and Na) are assumed to be fully hydrated and may completely shed their waters when sorbing on the surface (due to weak interaction with the surface). Cations such as K^+ and Cs^+ completely dehydrate during sorption and form strong ionic bonds with the surface. In caustic solutions, alkaline earth metals such as Sr do not fully hydrate ($Sr\text{-}OH^+$). Therefore, a strong (ionic) interaction with inorganic surfaces is expected. In contrast, anions are expected to strongly sorb on solid surfaces. The adsorption of anions is believed to occur via displacement of surface hydroxyls and the formation of mono and bidentate surface complexes with covalent bonding character. In SRS supernate, U and Pu exist as anion complexes of hydroxyls, carbonates, and nitrates. The hydroxyls in the complex can be displaced, and covalent bond formation with the surface oxygen is expected.

If the adsorption increases proportionally to the solute concentration, the adsorption process follows Henry's law. If the adsorption reaches a steady state value regardless of the solute concentration, then one can mathematically describe the adsorption process with a Langmuir equation (2, 3). For systems that exhibit other nonlinear increases in adsorption with solute concentration, several mathematical formulas can describe the adsorption process. Examples of nonlinear isotherms include Freundlich (4), Dubinin-Ashtakov (5–7), Tempkin (8), Volmer (9), Sips (10), Fowler-Guggenheim (11, 12), Frumkin-Damskin (13), Redlich-Peterson (14), Toth (15), Levan-Vermeulen (16), Vacancy Solute Theory (17), Radke-Prausnitz (18), Sigmoidal (19), General Adsorption Theory (20), Langmuir-Freundlich (21), Margules, Fowler-Guggenheim/Langmuir-Freundlich (22), Fowler-Guggenheim/Jovanovic-Freundlich (23), Jaroniec (22, 24), Ideal Adsorbed Solute Theory

(25–27), and Sheindorf-Rebuhn-Sheintuch (28). It is important to note that successfully fitting isotherms to adsorption data does not, in general, provide information about the mechanism of sorption. These expressions are best looked at as mathematical descriptors of the sorption data. However, the mathematical relations are useful for predicting and scaling adsorption operations. One must derive mechanistic details of sorption processes from other techniques such as surface spectroscopy (infrared, Raman, EXAFS, etc.).

We numerically optimized the parameters for the various published isotherms to available actinide and Sr adsorption data for sorption onto MST. We attempted to identify the best isotherm model that fit available data and reliably predicted MST performance as a function of MST and sorbate concentrations.

EXPERIMENTAL SECTION

Simulated and Actual Waste

We obtained the actinide and Sr data for simulated waste from previous research efforts and compiled the information into one data set (29–32). These experiments used the same basic protocols for studying the removal efficiency of MST at constant temperature. Most data come from work at ambient temperature (e.g., 25°C), although a few experiments examined performance at elevated temperatures (i.e., 45 and 65°C). Tests typically used solutions containing U, Sr, Pu, and Np in combination. Table 1 shows the range of concentrations studies. The experiments also examined removal performance as a function of solution composition and, to a more limited extent, for different manufacturing lots of MST. Table 2 shows the range of solution compositions included in the studies. The range of compositions shown in Table 2 represents the compositions of different tanks,

Table 1. Initial sorbate concentrations

Dataset	MST (g/L)	Sorbate equiv (μmole/L)	OH^- (M)	NO_3^- (M)	NA+ (M)
1	0.2, 1.1, 2.0	13–380	1.1–1.8	2.1–3.5	4.5–7.5
2	0.2, 0.4	51–99	2.4	1.1	4.5
3	0.2, 0.4	84	1.3	2.6	5.6
4	0.4	92–110	2.6	1.3	5.6
5	0.4	51–110	1–3	1–3	4.8–5.9

Table 2. Experimental compositions

Dataset	Sr	Pu	Np	U
1	5–100	1.1–280	340–36,000	1500–26,000
2	90	62	420	9000
3	87	190	420	9000
4	65–100	98–220	460–650	10,000–12,000
5	300–830	36–240	190–310	4300–10,000

their blends, and stimulant at SRS. The bottles were shaken in a temperature-controlled bath for finite lengths of time. At the end of the shaking, personnel filtered the solutions and analyzed the filtrate using Inductively Coupled Plasma Mass and Emission Spectroscopy, as well as analyzing for Pu by PuTTA separation (Pu^{238} and $Pu^{239/240}$ separation with 0.5 M thenoyltrifluoroacetone solvent followed by alpha spectroscopy detection) and radiocounting. We assumed that the loaded amount of actinide and Sr on MST equaled the difference between the original concentration in stock solutions and the final concentration in the bottles. The error associated with weighting MST equaled 5%. Propagation of errors calculation places the uncertainty in the actinide and Sr loading between 5 and 10% CV (Coefficient of Variation, or percent uncertainty).

The experimental data for actual and simulated wastes generally showed consistent agreement. However, the data sets do include considerable variance from a number of causes including the following:

- Extremely high mass or molar loadings of U on MST result in multilayer sorption behavior and a unique divergence from classical single monolayer isotherm forms.
- Nearly all the solutions contained U as the radionuclide with the highest mass concentration. The U data show the widest variance.
- The composite data set indicates a notable variance in sorption for different batches of MST. The sorption of Sr with different batches of MST shows the largest variance. This variance remains a relative unexplored aspect of the process design.

Further examination of the experimental data set identified additional data points measured at the detection limits of measuring instruments. The large variance of the data measured at detection levels places great uncertainty on the data in the isotherm. We eliminated data points measured at the detection limit from additional calculations. In the case of the Pu experimental points, only 60 out of 110 data points remained above detection limits. Further, we imposed an additional screening criterion on the maximum

radionuclide (i.e., sum of all four species) loading on MST allowed. The amount of sorbate should not exceed 2 μmole/g of MST. This criterion is based on the maximum expected number of equivalence MST can absorb by analogy with typical sorbents (33).

Similarly, the experimental data included a wide variety of solution compositions. As such, the mathematical expressions implicitly account for variances in solution chemistry typical of that anticipated within the Salt Waste Processing Facility and Actinide Removal Process. The reader must consider the ranges of these concentrations when applying the expressions.

Np Sorption

The fitting of experimental data to complex multicomponent models requires a number of decisions on the approach, some of which are subjective. We adopted two strategies for modeling the data. For each isotherm equation, we decided to fit all of the data simultaneously. Our second strategy constrained the parameter with the largest standard deviation. Large parameter deviations are typically due to limitations of the experimental design, the restricted size of the data sets, or an insufficient span of the data.

We evaluated the data for steady state (i.e., after 168 h) and mass balance consistency. We identified 29 different isotherm models for fitting to the data using JMP® software (version 5.0.1 from SAS Institute). The modeling generated correlation coefficients, sum of the squares of error (deviations from the mean) values (variance), "lack of fit," and significance probabilities for each isotherm. We used each of these criteria to rank the isotherms.

As a final criterion, we gave preference to those isotherms that provide a thermodynamically consistent representation of the data. In principle, such expressions hold a higher likelihood of extrapolating beyond the region of the original data used to obtain the parameters.

We ranked each isotherm expression separately for the performance relative to U, Pu, Sr, and Np. We summed the individual rankings, with equal weightings, for each criterion for each radionuclide.

An objective of this evaluation is the selection of one isotherm that can fit all four sorbates. We included, in this modeling effort, 110 data points from the simulated waste tests and 27 data points from the actual waste tests. As mentioned earlier, we omitted data points that either lacked mass balance consistency or that fell below the detection limit for a given radionuclide, or when the sum of masses for all the radionuclide exceeded our understanding of the available sorption sites on MST. The resulting number of data considered for Sr included 95 data points, for U 110 data points, for Pu 68 data points, and for Np 82 data points.

RESULTS AND DISCUSSION

Simulated and Actual Waste Modeling (Equilibrium Data)

We found three isotherm equations that reproduced the data in reasonably good fashion: the Fowler-Guggenheim-Jovanovich-Freundlich (FG-JF), Fowler-Guggenheim-Langmuir-Freundlich (FG-LF) and the Dubinin-Astashov (DA) isotherms. The DA model performed best per the selection criteria we defined. All three models replicated the nonclassical sorption behavior observed for U at extremely high mass loading resulting in an "upswing" in the curve associated with multilayer sorption behavior. Other models could not incorporate this behavior and simultaneously replicate data at lower mass loadings with practical error, or offset, from the experimental data. The FG-JF and FG-LF isotherms assume interactions between the adsorbed sorbates, between the solution and surface sorbates, and exponentially distributed surface energy sites on MST. The inclusion of many assumptions requires calculation of several parameters. On the other hand, the DA isotherm assumes an inverse Weibull distributed surface energy site on MST. The DA isotherm requires only four parameters to represent sorbate loading. We provide results from the FG-JF and DA isotherms (next) in this paper.

The DA isotherm equation incorporates this energy distribution as shown in Eq. (1). In Eq. (1), E represents the average adsorption energy. The parameter "S" represents the saturation limit of the radionuclide. The value Y_m represents the maximum radionuclide loading on MST.

$$Y = Y_m \exp\left[-\left(\frac{RT}{E}\right)^n \left(Ln\left(\frac{S}{X}\right)\right)^n\right] \tag{1}$$

We used a number of isotherm models to regress the plutonium adsorption data. Not all the isotherms successfully reproduced the data. We found the DA isotherm equation to fit the data well. We base our selection of the DA isotherm equation on the overall ranking using the criteria defined earlier [e.g., correlation coefficients, sum of the squares of error values (variance), "lack of fit" and significance probabilities for each isotherm, and the mathematical "simplicity factor"].

None of the ideal behavior isotherms such as Langmuir or the Ideal Adsorbed Solute theory (IAST) or Freundlich performed well. The FG-JF and FG-LF isotherm functions are mathematical combinations of the Fowler-Guggenheim, Langmuir, Jovanovic, and Freundlich isotherms. These isotherm equations include the interactions between loaded sorbents, between the loaded and free sorbate and surface heterogeneity. The successful prediction of the Pu, Sr, U, and Np data with the FG-JF and FG-LF models may indicate appreciable sorbate interactions and surface heterogeneity. On the other hand, the DA model successfully reproduced this data. The DA

model is based on the thermodynamic potential for adsorption (Gibbs energy) on sites with energies distribution described by a Weibull function. The DA isotherm successfully models filling of micropore spaces that occurs subsequent to the initial sorption layers. The DA model does not include loaded sorbate-to-sorbate interaction terms but has successfully fitted multilayer adsorption data. The successful fitting with the DA model reinforced the view of a heterogeneous MST surface. Since two different types of models (FG-JF or FG-LF and DA) successfully reproduced the data, we chose the model with the least number of variables and mathematical operations. Models with complex mathematical operations and numerous parameters exhibit large sensitivity to small variations. We recommend the DA model for further engineering calculations.

Plutonium Form of the DA Model

We fitted the Pu adsorption data at 25°C to all the isotherm equations mentioned before. We concluded that the DA model successfully fitted the Pu data. Figure 1 shows the DA isotherm for the 25°C results. Most of the data shown on Fig. 1 derives from simulant testing. The two data points at concentrations larger than 0.55 μM (i.e., 1757 nCi/g of ^{238}Pu or 6.4 nCi/g of ^{239}Pu) derived from actual waste testing. The actual waste data came

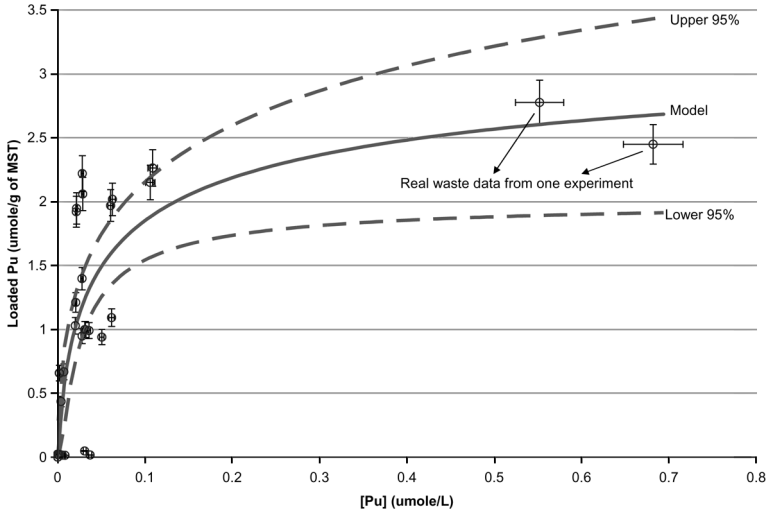

Figure 1. The prediction of the Pu data with the DA model. (Note: The data shown comes from experiments at 25°C.) The two data points above 0.55 μM are actual waste data. The waste data results from testing under unsteady conditions (i.e., only 14 h of testing).

from testing under nonsteady-state conditions (i.e., after only 24 h of sorption testing). Glancing at Fig. 1, the DA model successfully explained 72% of the variance (correlation coefficient, $R^2 = 0.72$) in the Pu adsorption data (the correlation coefficient is the proportion of the variance that can be attributed to a linear relationship between the model and the data). Note the relatively large data scatter at Pu concentrations less than 0.1 μM. The scatter represents the collection at several different experimental conditions. To ensure accurate calculation of the parameters in the model, the data must include the initial rise and plateau (i.e., saturation) of the loading final concentration curve. Figure 1 shows a large compilation of data at the initial rise of the curve and only two points at the plateau of the curve. The two data points at a Pu concentration of 0.55 (i.e., 1757 nCi/g of ^{238}Pu or 6.4 nCi/g of ^{239}Pu) and 0.7 μM (i.e., 2236 nCi/g of ^{238}Pu or 8.14 nCi/g of ^{239}Pu) originated from one adsorption experiment terminated 24 h after initiation of sorption testing. Therefore, the proposed calculated parameters depend heavily upon the accuracy of these two data points. The additional two dashed-line curves are the 95% prediction confidence curves. The predictions curves agree well at low Pu concentrations and diverge widely at high Pu concentrations. The large variance in the 45 and 65°C data resulted in a poor fitting with the DA model. In general, the amount of Pu loaded on MST at 45 and 65°C proved lower than at 25°C.

The DA equation for Pu loading on MST at 25°C is shown in Eq. (2). In Eq. (2), the temperature is in units of Kelvin, and the Pu concentration unit is in micromoles per liter. Note the value of the exponent for both the concentration and temperature equals 2. A value of 3 or less is typically assigned to a narrow energy distribution for sorption sites. The surface homogeneity assumed from the DA model is not consistent with previous microscopy and spectroscopy analysis of MST. The value 0.0008 (which equals the "a" parameter) equals to the gas constant divided by the average adsorption energy (R/E) raised to the "nth" power and in this the 2nd power. From this expression, we calculated the average adsorption energy "E." The calculated average adsorption energy from the previous expression equals 294 J/mole. This energy is well below the adsorption energy of Sr on clay (typically 7 kJ/mole) (34). The low sorption energy value explains the ease of actinide sorption on MST. The energy of ion exchange reactions typically ranges from 8 to16 kJ/mol. The calculated energy value of 294 J/mole indicates the mode of adsorption is specific (or multilayer), in agreement with recent XAFS findings.

$$Loaded\ Pu = (2.6 \pm 0.5) \times \exp\left(-(3 \pm 2 \times 10^2)^{2\pm1} \times \left[Ln\left(\frac{0.8 \pm 1.2}{[Pu]}\right)\right]^{2\pm1}\right) \quad (2)$$

We fitted the three temperature data sets simultaneously with the DA function. The DA model explained 74% of the variance in the data (26% not explained by the linear relationship between DA model and the data). The DA equation for Pu loading on MST is shown in Eq. (3). In Eq. (3), the larger parameter uncertainty is due to additional data scatter from the wider temperature range tested. The parameter listed before the temperature variable and the parameter in the logarithm term may not be statistically significant. The model predicts loading decreases with increasing temperature. Raising the temperature during sorption provides additional thermal energy for the loaded Pu to desorb. Please note testing included only three temperatures. We recommend this expression for predicting Pu loading on MST within the temperature range evaluated in this study.

$$Loaded\ Pu = (471 \pm 174) \times \exp\left(-.27 \pm .14 \times Temperature^{0.4 \pm .02} \times \left[Ln\left(\frac{3.6 \pm 9}{[Pn]} \right) \right]^{0.4 \pm .02} \right) \quad (3)$$

Regression of the data for the Pu loading equation resulted in a significant uncertainty in the parameter values. For example, the uncertainty of the "S" parameter is three times larger than the estimated value. The "S" (previously identified as the shape factor for a Weibull distribution) parameter stands for the solubility limit of the nuclide in solution. To determine how sensitive the DA equation is to parameters variations, we computed and graphed the sensitivity factors for each of the coefficients. Figure A1 in Appendix A contains the sensitivity plots.

Strontium Form of the DA Model

We fitted the Sr loading data to the isotherm models. We concluded that the DA model successfully fitted the Sr data. Figure 2 shows the loading data, as well as the DA model prediction for Sr sorption at 25°C. Again, the large variance of the 45 and 65°C precluded fitting with the DA model at these two temperatures alone. The DA model explained 97% of the data variability ($R^2 = 0.97$). The data scatter at [Sr] < 0.1 M is due to different experimental conditions tested in the adsorption experiments. The DA model reproduced this scatter by including the effects of temperature. In Fig. 3, the points represented by the filled circles are DA model predictions. The final DA isotherm equation presents a heterogeneity value ("n") of 1. The site energy distribution is very narrow. The surface of MST appears very homogeneous

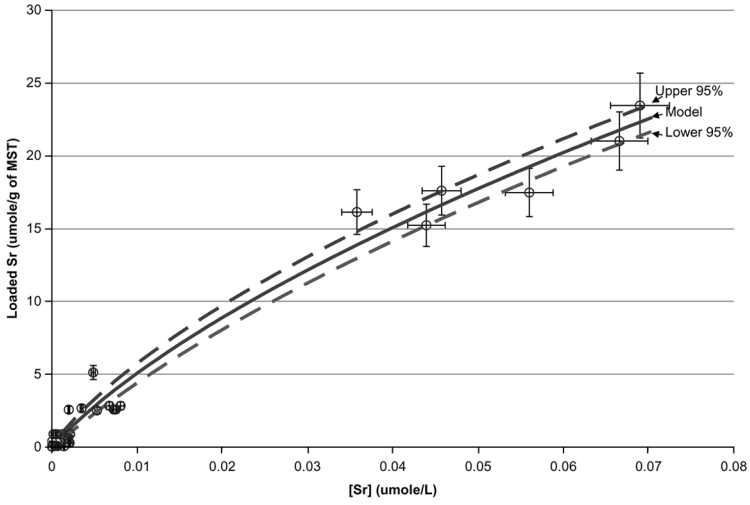

Figure 2. The DA model predictions for the Sr loading data at 25°C. The confidence limits are for the mean response. Please note the error bars on the data.

for Sr adsorption. The average adsorption energy, as predicted by the DA model, is 3.3 kJ/mole. This enthalpic energy is above the energy available at room temperature (2477 J/mole) for Brownian motion. Therefore, the Sr sorption is irreversible. The inverse Weibull statistics indicate that, to

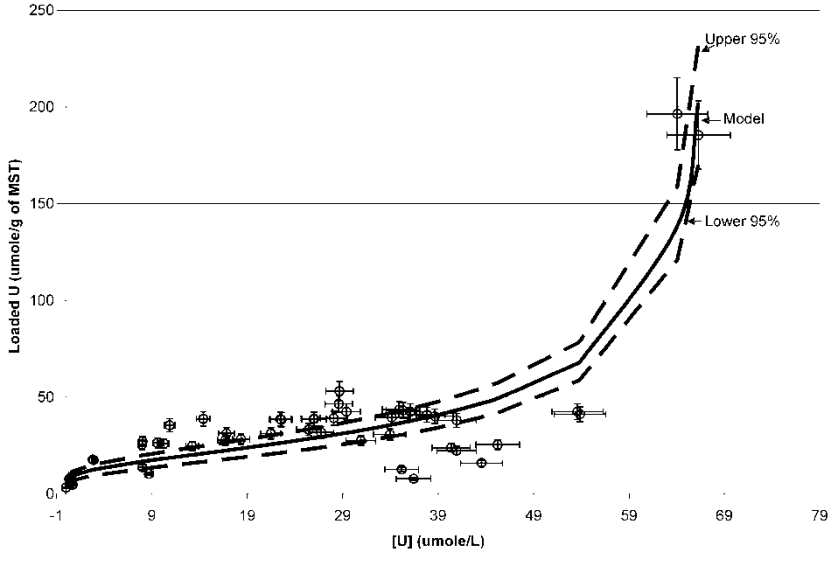

Figure 3. The DA model fit of the U data at 25°C.

maximize the specific loading, the energy must be as large as possible. Also, from the DA equation, the maximum Sr loading on MST is predicted to be 31 micromoles per gram of MST (e.g., the pre-exponential term in the following equation) at a 95% confidence level. No experimental measurement of the maximum Sr loading on MST has been made to date for comparison. To convert from μmol/L of Sr-90 to nCi/g of solution multiply the μmol/L unit by 9960 (assuming a solution density of 1274 g/L).

The corresponding DA equation for Sr at 25°C is shown in Eq. (4). The "$\pm$" terms in the equations represent the standard error for the parameters. Since they have strong correlations with the other parameters, the pre-exponential and the logarithm parameters may not be statistically significant. We also fitted the data for all three temperatures simultaneously yielding Eq. (5). The DA model equation for Sr loading follows with the same units as used for Pu. Note at 298°K both Eqs. (5) and (6) predictions differ, suggesting additional work is needed. We recommend Eq. (6) for Sr loading predictions. The sensitivity plots for this equation are shown in Fig. A2 of Appendix A.

$$Loaded\ Sr = 22 \pm 19 \times \exp\left[-(6.8 \pm 2 \times 10^2)^{1 \pm .33} \times \left(Ln\left(\frac{0.07 \pm .12}{[Sr]} \right) \right)^{1 \pm .33} \right] \tag{4}$$

$$Loaded\ Sr = 410 \pm 138 \times \exp\left[-0.09 \pm 0.02 \times Temperature^{0.55 \pm .009} \times \left(Ln\left(\frac{0.42 \pm .12}{[Sr]} \right) \right)^{0.55 \pm .009} \right] \tag{5}$$

Uranium Form of the DA Model

We fitted the different isotherm functions to the U adsorption data. Again, we concluded that the DA model successfully fitted the U data especially at high U loadings, where the other models failed to predict. For this reason, we selected the DA model to represent the loading behavior of all three radionuclides. Figure 3 shows the experimental loading data, as well as the DA model predictions at 25°C. Figures 4 and 5 show similar predictions for the 45 and 65°C data. Figure 6 shows the results for the DA model with parameters regressed simultaneously for the entire data set. The loading data display a take off or "tail" at [U] $>$ 65 micromoles/L. This likely indicates

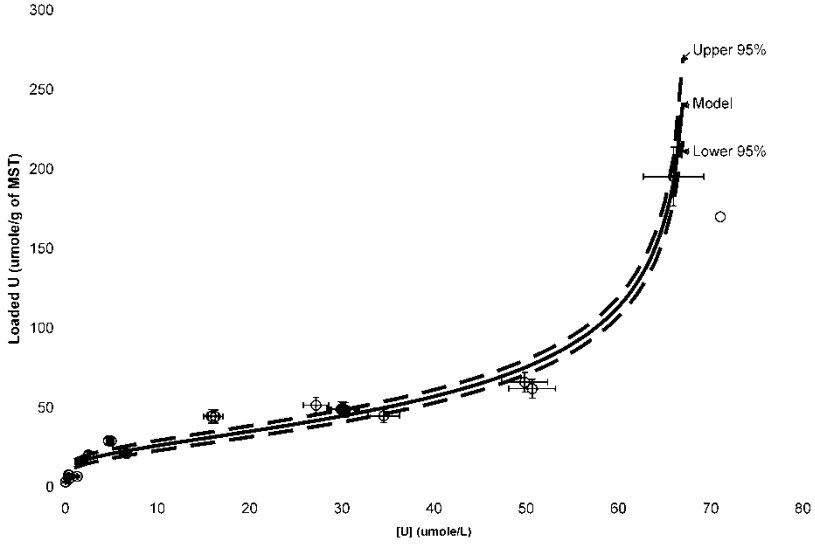

Figure 4. The DA model results and the 45°C U absorption data.

multilayer formation as originally suggested by previous scattering spectroscopy work. The feature of the DA model in reproducing the upper "tail," or "upswing," suggests formation of chemical networks throughout the micropore space. If the DA model assumptions are correct, then the

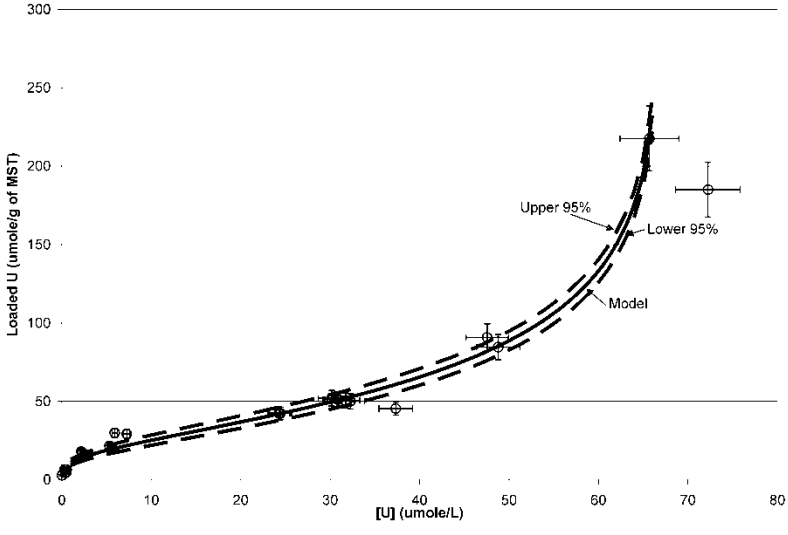

Figure 5. The DA model for the 65°C U data.

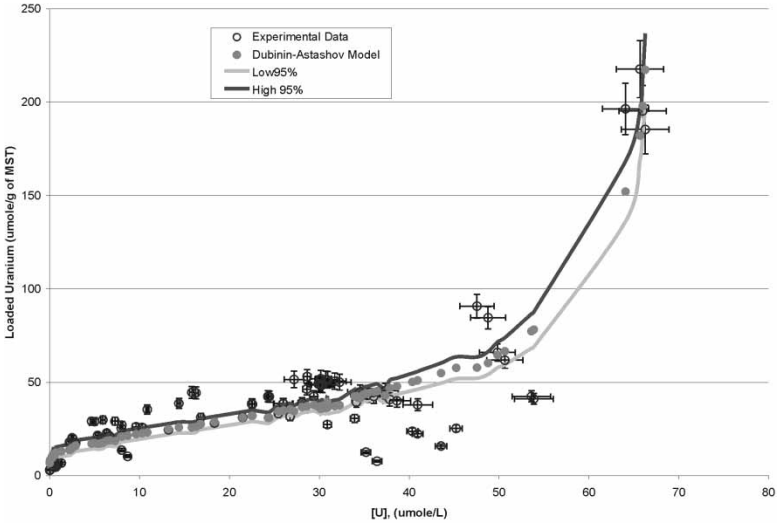

Figure 6. The U loading data on MST at 25°C, 45°C, and 65°C. The figure also includes the DA predictions.

sites energy distribution on MST is very narrow and homogeneous (as indicated by the "n" value of 0.16).

The average adsorption energy on MST is very low, about 5 J/mole. The magnitude of this energy indicates multilayer formation. Note the parameter listed before the temperature variable in Eq. (6) may not be statistically significant. The DA model predicts MST can adsorb 1,865 micromoles of U per gram of MST (or 44 wt %). The previously experimentally determined maximum loading is 1.28 wt % (30). The predicted maximum loading is 34 times the experimental value. We recommend additional testing at large U concentrations (>100 umole/L) to accurately determine the maximum capacity of MST for fissile uranium. This information is essential for developing the safety bases for the operations. The DA isotherm equation for U loading that includes the three temperatures tested is shown in Eq. (6) using the same units as stated earlier. The sensitivity plots for the coefficient of this equation are shown in Fig. A3 of Appendix A.

$$Loaded\ Uranium = 1865 \pm 472 \times \exp\left[-20 \pm 15 \times Temperature^{0.16 \pm .01} \times \left(Ln\left(\frac{68 \pm 0.3}{[U]} \right) \right)^{0.16 \pm 0.001} \right] \quad (6)$$

Neptunium Form of the DA Model

We organized the Np data according to temperature and plot it in Fig. 7. Inspection of data in Fig. 7 shows that higher adsorption occurred at higher temperature. This observation is contrary to the temperature dependency of U, Pu, and Sr. This temperature behavior may be due to surface nucleation and precipitation. The DA equation for the Np sorption data at 25°C is shown in Eq. (7). A summary of the DA model's parameters for all three radionuclides is shown in Table 3. The low U adsorption energy on MST is due to surface precipitation.

$$Loaded\ Np = 64.9 \pm 9 \times \exp\left[-(0.6 \pm 0.3)^{1.1\pm.5}\left(Ln\left(\frac{75.3 \pm .01}{[Np]}\right)\right)^{1.1\pm.5}\right] \quad (7)$$

The Effect of Excess Uranium Loading on Pu, Sr, and Np Loading

Figure 8 shows the U, Np, Sr, and Pu data side by side. Looking at the U plot in Fig. 8, the data at large loadings (indicated by the symbol "X" in both figures) correlate with the large Pu loading (shown with the symbol

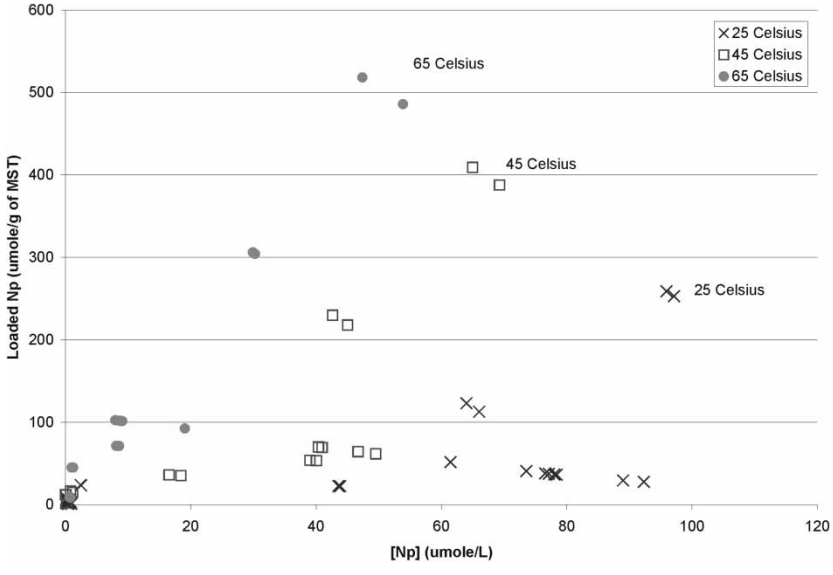

Figure 7. The Np loading data on MST at 25°C, 45°C, and 65°C.

Table 3. A summary of the Dubinin-Astashov parameters found for the radionuclides

Component	Maximum loading (μmole/G of MST)	Saturation limit (μmole/L)	Exponent value	Calculated adsorption energy (J/mole)
Pu-25°C	2.6 ± 0.5	0.83 ± 1.2	2.1 ± 1.5	238
Pu-25, 45, and 65°C	471 ± 173	3.6 ± 9.2	0.41 ± 0.02	202
Sr-25°	23 ± 25	0.07 ± 0.12	1.1 ± 0.28	1929
Sr-25, 45, and 65°C	410 ± 138	0.42 ± 0.11	0.55 ± 0.01	662
U-25°C	4845 ± 1266	67.8 ± 0.46	0.126 ± 0.01	2E − 10
U-25, 45, and 65°C	1866 ± 472	68 ± 0.3	0.16 ± 0.008	6E − 8
Np-25°C	65 ± 9	75.3 ± 0.01	1.1 ± 0.5	4437

Note the fitting with the Np data at 25°C was poor. No successful fitting was possible with the Np data at three different temperatures.

"X") shown in the Pu figure. This may be evidence of coprecipitation or specific adsorption on deposited U. Since the final Pu concentration fell below the detection limit, we eliminated the Pu data at this loading. At the same time Np also largely loaded on MST, while Sr did not load to the

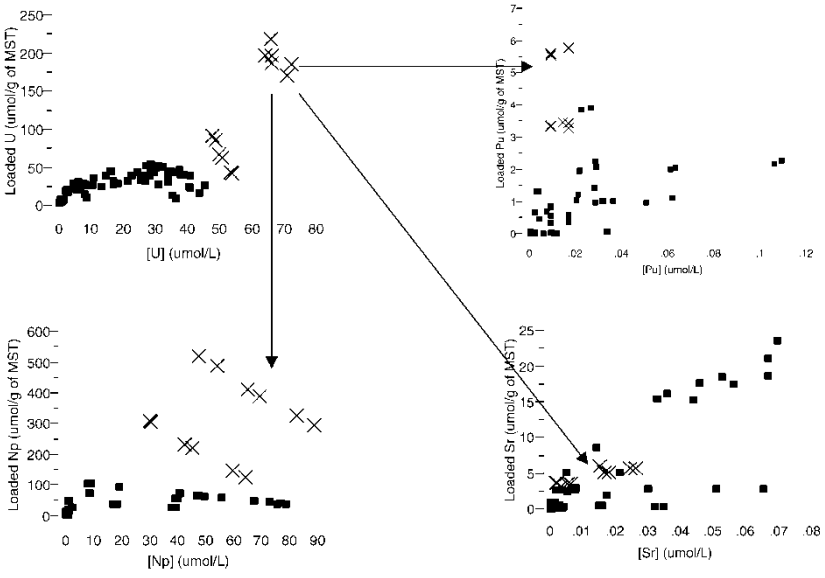

Figure 8. The effect of excess U loading on the Np, Sr, and Pu loading.

same extent. The large U sorption appears to enhance both Pu and Np loading and inhibits Sr loading.

CONCLUSIONS

We identified 3 models, out of 29 examined, that can fit and predict U, Sr, and Pu loading on MST. Two of the models—the FG-JF and FG-LF—are inverse models. The DA model is a conventional isotherm. We recommend the DA model for its minimal amount of parameters and for ease of application. The DA model successfully reproduced the U, Sr, and Pu data set. The binding energies derived from the model explain the observed irreversibility of the adsorption process on MST.

To enhance our predictive tools, we recommend additional testing that includes wider range of actinide and Sr concentrations, verifying in particular the limited data set for high Pu concentrations. We also recommend adding Am and Cm to future experimental studies to expand our data set on these two actinides.

We recommend a more complete analysis of the implications that increased U trapping in the micropores has on facility operation and risk of nuclear criticality.

We recommend continuing the modeling analysis for nonequilibrium data at shorter processing times. Analyzing this data offers the greatest benefits for assessing options to accelerate production rate for the facilities.

We also recommend additional testing of single component and binary actinide solutions. These studies will either verify the parameters found from the multicomponent study or indicate the need to explicitly develop the forms of the model that show binary interaction.

APPENDIX A. SENSITIVITY PLOTS FOR THE DA ISOTHERM EQUATION

Sensitivity plots for the DA isotherm equation's coefficient for three radionuclide follows. In Figs. A1–A3, the ordinate variable is the Sum of Squares of the Error (SSE). Recall that SSE is the deviation or distance between the model at current parameter values and the data. In the four graphs shown in Figs. A1 to A3, we changed only one variable at a time (shown in the coordinate scale), while keeping the other variables at the optimized values. Inspection of Figs. A1 to A3 reveals the most sensitivity parameters are "Y_m" (maximum loading, the preexponential term in the equation above) and the value "a," associated with the specific adsorption energy of the sites on MST. The parameter "a" is equivalent to the parameter "E" mentioned earlier. A significant increase in the SSE values

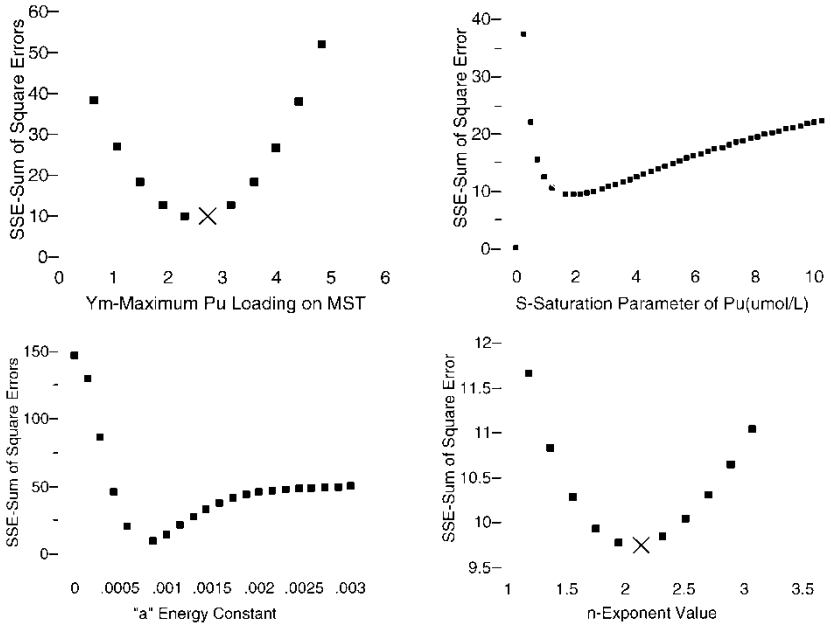

Figure A1. Sensitivity plots of the DA parameters determined from the Pu data at 25°C.

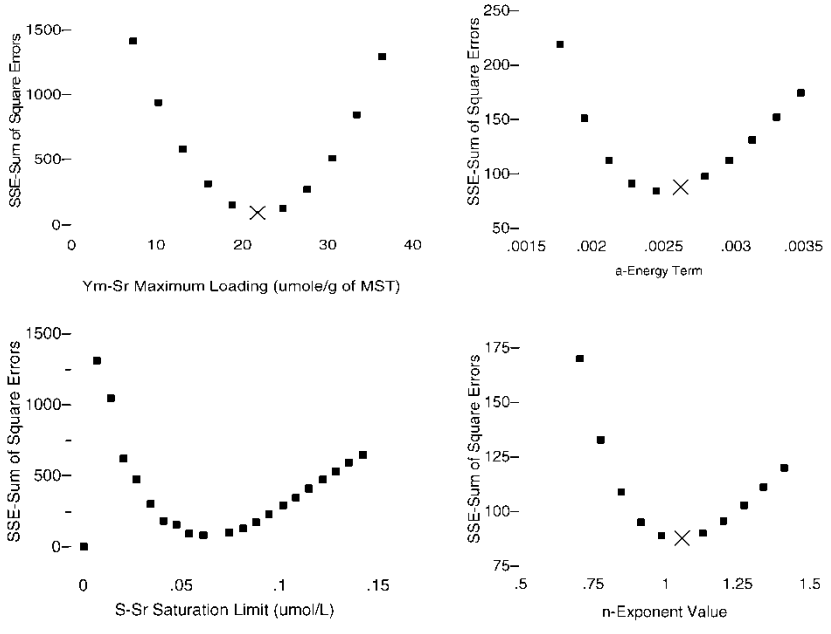

Figure A2. The sensitivity graphs of the DA model for the Sr loading data (at 25°).

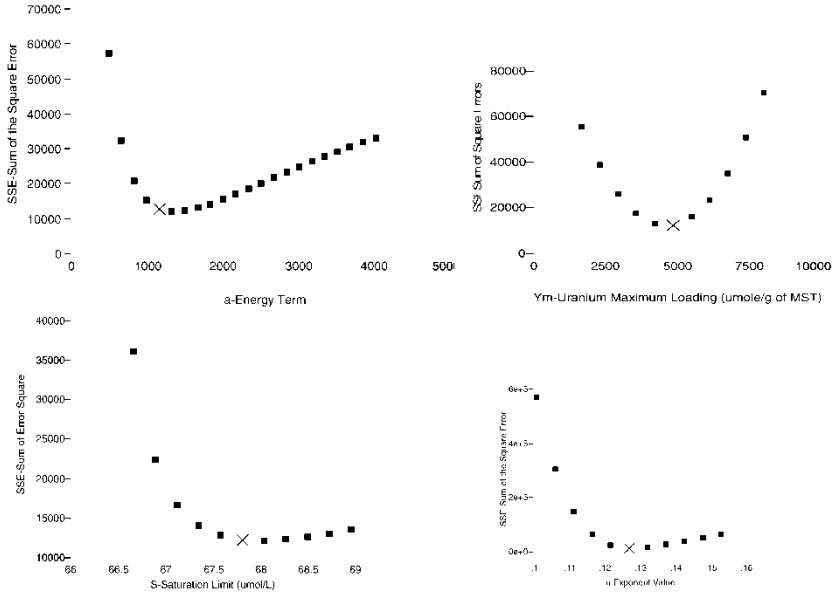

Figure A3. Sensitivity plots of the DA isotherm for U.

with small changes in the "Y_m" and "a" occurs. In Fig. A1, the optimal parameter is at the minimum value of SSE. For example, looking at the SSE vs. "n" subfigure the data point marked with a red "X" symbol is the value of "n" used in the Pu isotherm equation.

REFERENCES

1. Duff, M.C., Hunter, D.B., Hobbs, D.T., and Fink, S.D. (2001) *Characterization of Sorbed Strontium on Monosodium Titanate*; Westinghouse Savannah River Center—Technical Report-2001-00245, 1–16.
2. Langmuir, I. (1918) The Adsorption of Gases on Plane Surfaces of Glass, Mica and Platinum. *J. Am. Chem. Soc.*, 40: 1361–1368.
3. Butler, J.A.V. and Ockrent, C. (1930) Studies in Electrocapillarity. Part III. The Surface Tensions of Solutions Containing Two Surface Containing Two Surface Containing Two Surface-Active Solutes. *J. Phys. Chem.*, 34: 2841–2845.
4. Freundlich, H.M. (1906) *J. Phys. Chem.*, 57: 385–470.
5. Dubinin, M.M. and Radushkevich, L.V. (1947) Equation of the Characteristic Curve of Activated Charcoal. *Chem. Zentr*, 1: 875–889.
6. Dubinin, M.M. and Radushkevich, L.V. (1966) Evaluation of Microporous materials with a New Isotherm. *Dokl. Akad. Nauk SSSR*, 55: 331–347.
7. Dubinin, M.M. and Astakhov, V.A. (1970) 2nd Int. Conf. on Molecular-Sieving Zeolites, 43–57.

8. Tempkin, M.J. and Pyzhev, V. (1940) Recent Modifications to Langmuir Isotherms. *Acta Physiochim USSR*, 12: 217–225.
9. Ruthven, D.M. (1984) *Principles of Adsorption and Adsorption Processes*; J. Wiley: New York.
10. Rounsley, R.R. (1961) Benzene Adsorption on Activated Carbon. *AIChE J.*, 7: 308–314.
11. Fowler, R.H. and Guggenheim, E.A. (1939) *Statistical Thermodynamics*; MacMillan: New York, 430–433.
12. Kaczmarski, K. and Antos, D. (1999) Calculation of Chromatographic Band Profiles with an Implicit Isotherm. *J. of Chromatography A*, 862: 1–16.
13. Frumkin, A.N. (1925) A Multicomponent Isotherm for Gas Adsorption. *Z. Phys. Chem.*, 116: 466–472.
14. Relich, O. and Peterson, D.L. (1959) A Useful Adsorption Isotherm. *J. Phys. Chem.*, 63: 1024–1029.
15. Toth, J. (1971) A Multicomponent Isotherm for Liquid Adsorption. *Acta Chim. Acad. Sci. Hung.*, 69: 311–322.
16. LeVan, M.D. and Vermeulen, T. (1981) Binary Langmuir-Like and Freundlich Isotherms for Ideal Adsorbed Solutions. *J. Phys. Chem.*, 85: 3247–3250.
17. Suwanayuen, S. and Danner, R.P. (1980) A Gas Adsorption Isotherm Based on Vacancy Solution Theory. *AIChE J.*, 26: 68–76.
18. Radke, C.J. and Prausnitz, J.M. (1972) A New Adsorption Isotherm for Heterogeneous Surfaces. *Ind. Eng. Chem. Fund.*, 4: 445–457.
19. Meghea, A., Mihalache, R., Bumbac, G., and Constantinescu, I. (1994) Recent Developments in Isotherm Adsorption. *Sci. Techn. Env. Protection*, 3: 10–19.
20. Buckman, N.G., Hill, J.O., and Magee, R.J. (1983) A New Adsorption Isotherm for Gases. *Microchem. J.*, 28: 470–492.
21. Sposito, G. (1980) Derivation of the Freundlich Equations for Ion Exchange Reactions in Soils. *Soil Sci. Soc. Am. J.*, 44: 652–659.
22. Jaroniec, M. and Madey, M. (1998) *Physical Adsorption on Heterogeneous Solids*; Elsevier: Amsterdam.
23. Quinones, I. and Guiochon, G. (1998) Isotherms for Liquid Adsorption Systems. *J. Chromatogr. A*, 15: 796–811.
24. Jaroniec, M. and Toth, J. (1976) Modifications to the Langmuir Isotherm: Extension to Multicomponent Adsorption Systems. *J. Colloid Polym. Sci.*, 254: 643–652.
25. Porter, J.F., McKay, G., and Choy, K.H. (1999) The Prediction of Sorption from a Binary Mixture of Acidic Dyes Using Single- and Mixed-Isotherm Variants of the Ideal Adsorbed Solute Theory. *Chem. Eng. Sci.*, 54: 5863–5885.
26. Myers, A.L. and Prausnitz, J.M. (1965) Thermodynamics of Mixed-Gas Adsorption. *AIChE J.*, 11: 121–127.
27. Radke, C.J. and Prausnitz, J.M. (1972) Thermodynamics of Multi-Solute Adsorption from Dilute Liquid Solution. *AIChE J.*, 18: 761–768.
28. Sheindorf, C., Rebhum, M., and Sheintuch, M. (1981) A Freundlich-Type Multicomponent Isotherm. *J. Colloid Interface Sci.*, 79: 136–142.
29. Hobbs, D.T., Bronikowski, M.G., Edwards, T.B., and Pulmano, R.L. (1999) *Final Report of Phase III Testing of Mono-Na Titanate Adsorption Kinetics*; Westinghouse Savannah River Center—Technical Report-99-00134.
30. Hobbs, D.T. and Ulmano, R.L. (1999) *Phase IV Simulant Testing of Mono-Na Titanate Adsorption Kinetics*; Westinghouse Savannah River Center—Technical Report-99-00219.

31. Hobbs, D.T. (2000) *Phase V Simulant Testing of Monosodium Titanate Adsorption*; Westinghouse Savannah River Center—Technical Report-2000-00142.
32. Hobbs, D.T. (2001) *Solution Composition and Alternate Materials*; Westinghouse Savannah River Center Technical Report-2001-00436.
33. Hobbs, D.T. and Fleichman, S.D. (1992) *Fissile Solubility and MST Loading Test*; Westinghouse Savannah River Center Report-92-1273.
34. Atun, G. and Kaplan, Z. (1996) Influences of Salt Concentration, Loading and pH on Strontium Adsorption. *J. Radioanal. Nucl. Chem. Art.*, 211 (2): 425–434.